Numerical Modeling of Separated Flows at Moderate Reynolds Numbers Appropriate for Turbine Blades and Unmanned Aero Vehicles

By G. Castiglioni, J. A. Domaradzki, M. Grilli† AND S. Hickel†

Department of Aerospace Engineering
University of Southern California
Los Angeles, CA 90089-1191, U.S.A.

Flows in rotating machinery, for unmanned aerial vehicles (UAV), micro air vehicles (MAV), wind turbines, and propellers are often dominated by the effects of flow separation. Such effects can greatly influence lift and drag, and thus flight stability of UAV's, efficiency of wind turbines, and unsteadiness in turbine flows which is instrumental in predicting high cycle fatigue (HCF) for turbomachinery components. In order to produce efficient designs or control schemes to reduce separation effects, efficient numerical prediction tools for such flows are needed. Low Reynolds number separated flows have been simulated using direct numerical simulations (DNS), large eddy simulations (LES), and Reynolds averaged Navier-Stokes equations (RANS). While both RANS and LES are able to predict some features of such flows, only DNS are currently considered to be capable of predicting all features, including the separation point. However, this comes at a considerable computational cost, making DNS not feasible in industrial practice. The goal of this project is to investigate the ability of LES techniques to predict separated flows at resolutions by a factor of 100 less than in DNS. The geometrical setting is that of a 3D airfoil at incidence for which detailed DNS results are available. We have performed simulations of a laminar separation bubble on a NACA-0012 airfoil at $Re_c = 5 \times 10^4$ at 5 deg of incidence with resolution reduced drastically from that used in DNS. The results to date show good predictions for the pressure coefficient C_p and the separation point, but poor comparison with DNS data for the friction coefficient C_f, indicating that further work is needed to achieve the stated goals of the project.

1. Introduction

Reynolds numbers for flows in rotating machinery, for unmanned aerial vehicles (UAV), micro air vehicles (MAV), wind turbines, and propellers are usually low or moderate. Based on wing/blade chord they are typically less than 2×10^6 and often only on the order of few $10^4 \ - \ 10^5$. By comparison, civilian aeroplanes are characterized by the Reynolds numbers ranging from few millions to 80×10^6 for the Boeing 747 at cruising velocity. There is a long history of research on high Reynolds number aerodynamics, driven by its importance in the aerospace industry, and there exist robust numerical tools for the prediction of lift and drag forces for streamlined bodies. The recent experimental investigations of low Reynolds number aerodynamics [1–3] reveal new features

† Lehrstuhl für Aerodynamik und Strömungsmechanik, Technische Universität München, Boltzmannstr. 15, 85748 Garching b. München

of such flows that complicate their prediction compared with high Reynolds number flows. Aerodynamics at moderate and low Reynolds numbers is less developed, partly because the field was less important before, but mostly because of a unique physical difficulty: such flows are often dominated by the effects of flow separation. The flow separation can greatly influence lift and drag, and thus flight stability of UAV's, efficiency of wind turbines, and unsteadiness in turbine flows which is instrumental in predicting high cycle fatigue (HCF) for turbomachinery components. In order to produce efficient designs or control schemes to reduce separation effects we need prediction tools for such flows. However, while there are experimental data on both the time-averaged lift and drag forces and the instantaneous flow fields over wings, the agreement between different experiments is often poor, indicating that the separation process can be sensitive to details of experimental setups.

The physical origin of the observed behavior is qualitatively well understood: it is caused by a sudden appearance of the laminar separation bubble that changes the flow pattern around a wing and thus its properties. The main features of the laminar separation bubble are illustrated in Fig. 1 taken from [4]. The attached laminar boundary layer developing on a wing is subjected to an adverse pressure gradient due to the wing curvature that causes it to separate. Immediately behind the separation point there is an effectively stagnant flow region, the so-called "dead air" region, followed by a reverse flow vortex. The interface between the separated flow moving away from the wing and the recirculating flow in the vicinity of the wing results in a shear layer with an inflectional mean velocity profile. This shear layer experiences Kelvin-Helmoholtz instabilities, developing into turbulence, after generating first characteristic spanwise vortices. Further downstream the separated turbulent flow reattaches and gradually evolves into the classical turbulent boundary layer. The above picture emerges from numerous experimental investigations, e.g., [1–3] as well as from direct numerical simulations (DNS) results [4–9]. Note that despite the fact that the term "laminar" is used, the actual flow is a mixture of regions where the flow is laminar, transitional, non-equilibrium turbulent boundary layer, and an equilibrium turbulent boundary layer.

The agreement between experiments and computations is even harder to find, indicating potential difficulties in developing separation prediction tools. This is because the separation process, especially driven by adverse pressure gradient as opposed to geometry, is essentially non-equilibrium, involving subtle interactions between viscous, advective, and pressure effects that can be captured only by full Navier-Stokes equations. Indeed, at present the reliable numerical results for such flows have to be obtained using direct numerical simulations (DNS). However, such DNS require substantial computational resources, long wall-clock runs and long analysis times, e.g., [6] used over 170 million grid points for a relatively simple 3-D configuration. Such numerical simulations of full N-S equations are not feasible if number of configurations and angles of attack are to be investigated. Therefore, other simulation options must be considered. One option is to employ RANS models, modified to account for the reduction of the eddy viscosity around the separation region. This is approach commonly used and optimized for high Reynolds number, turbulent flows, but not as useful for the separated flows of interest. Another option is to employ LES techniques. For instance, Yang and Voke [10] reported LES results obtained with the dynamic Smagorinsky model in a good agreement with experiments for boundary-layer separation and transition caused by surface curvature at $Re = 3,450$. Yet even for this relatively low Reynolds number, the critical issues in getting the agreement was good numerical resolution (472x72x64 mesh points)

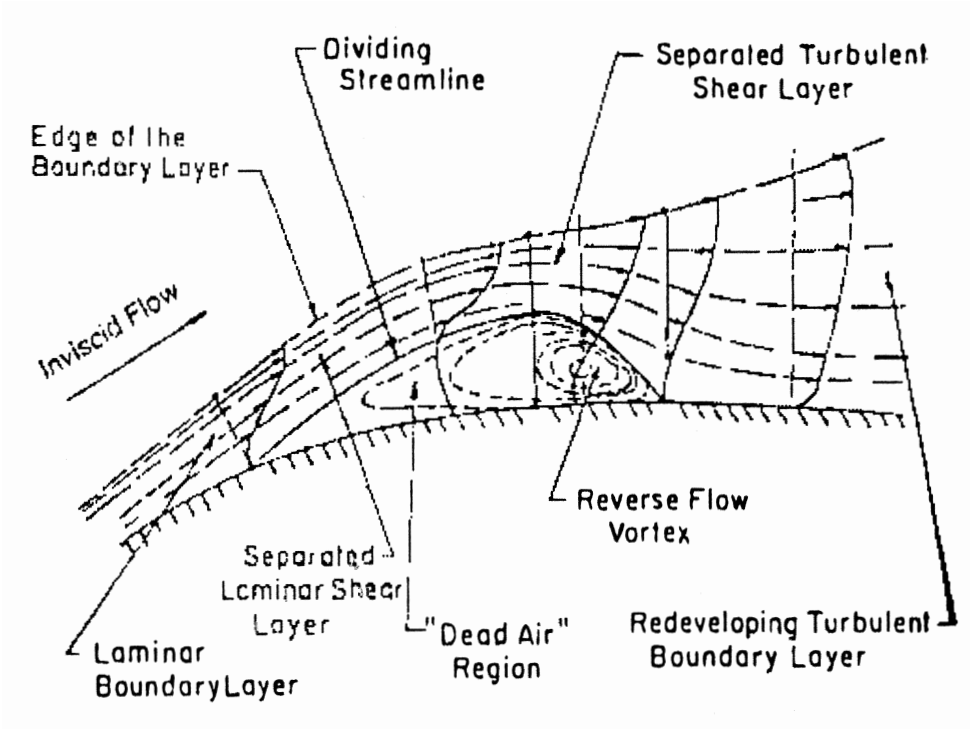

FIGURE 1. Features of a laminar separation bubble flow (after [4]).

and high order numerical method, requirements difficult to satisfy in simulations of practical flows often performed with low order finite difference or finite volume methods (e.g., commercial codes). Similarly, Eisenbach and Friedrich [11] performed LES of flow separation on an airfoil at high angle of attack at $Re = 10^5$ using cartesian grids. This case also required very high resolutions between 50 and 100 million mesh points.

Here we report on an initial study of a separation problem for a flow around a wing/blade at moderate Reynolds numbers using LES. The specific geometrical setting is that of a 3D airfoil at incidence for which detailed DNS results were obtained in [6, 7]. The goal of the project is to reproduce the laminar separation bubble on a NACA-0012 airfoil at $Re_c = 5 \times 10^4$ at 5 deg of incidence with *resolution reduced drastically from that used in DNS and typical LES performed for this problem*. The reduction target is a factor of 100. To simulate this case the code developed at TUM that uses immersed boundary method (IB) has been employed. While the code is designed to simulate 3-D flows we have performed only 2D simulations to date. This work is to be considered as a test case: if the laminar separation bubble problem can be correctly resolved, the long-term goal would be to simulate the flow around progressively more complex geometries (a turbine blade, turbine stator/rotor and full stage). The use of the IB code will significantly facilitate the simulation of more realistic and complex geometries in comparison with a standard finite volume curvilinear code.

2. Numerical method

2.1. *Governing equations*

The numerical code solves the compressible three-dimensional Navier-Stokes equations in conservative form. The solution vector contains the volume-averaged density ρ, momentum ρu_i and total energy ρE. We assume the fluid to be a perfect gas with a Prandtl number of $Pr = 0.72$ and a specific heats' ratio of $\gamma = c_p/c_v = 1.4$. The governing non-dimensional flow parameters are the Reynolds number Re and the Mach number Ma. Pressure and temperature are then determined by the ideal-gas equation of state (EOS)

$$p = \frac{1}{\gamma Ma^2}\rho T \tag{2.1}$$

and the definition of the internal energy

$$\rho e = \rho E - \frac{1}{2}\rho u^2 = \frac{1}{\gamma - 1}p\ . \tag{2.2}$$

A power law is assumed for the temperature dependence of viscosity

$$\mu = \frac{1}{Re}T^{0.75} \tag{2.3}$$

and thermal conductivity

$$\kappa = \frac{1}{(\gamma - 1)Ma^2 Pr}\mu(T)\ . \tag{2.4}$$

2.2. *Grid and boundary conditions*

The generation of suitable grids for LES of complex flows can be time-consuming and difficult. Contradictory requirements, such as adequate local resolution and minimum number of grid points, can deteriorate the grid quality and adversely affect accuracy and numerical convergence properties. We use Cartesian grids, which facilitate automatic grid generation and adaptive local grid refinement by dyadic sub-partitioning. Cartesian grids also imply fewer computational operations per grid point than body-fitted or unstructured grids. On the other hand, geometric boundaries do not necessarily coincide with grid lines, so that boundary conditions have to be applied at the subcell level.

We use a conservative immersed boundary method for representing sharp interfaces between a fluid and a rigid body on Cartesian grids, see Refs. [12, 13]. A level-set technique is used for describing the interface geometry. The level-set function is the signed distance between each point in the computational domain and the immersed interface, which is positive within and negative outside of the fluid domain. The zero contour is the interface between the fluid and the obstacle. The intersection of the obstacle with the Cartesian grid produces a set of cells that are cut by the interface. The underlying finite-volume discretization is modified locally in these cut cells in such a way that it accounts only for the fluidic part of a cell. Required interface normals, face apertures and fluid-volume fractions of cut cells can be computed efficiently from the level-set function. The viscous stresses at the fluid-solid interface are approximated by linear differencing schemes. The interface pressure is obtained by solving the one-sided (symmetric) Riemann problem in the interface-normal direction.

As we operate on fluxes only, this cut-cell finite-volume method maintains accuracy and ensures mass and momentum conservation. Discrete conservation and a sharp

representation of the fluid-solid interface render our method particularly suitable for LES of turbulent flows.

Characteristic boundary conditions of Poinsot and Lele [14] are applied at the far-field domain boundaries. At the downstream exit boundary, which will be subject to the passage of nonlinear fluid structures, a low value for the reflection parameter has been set. These boundary conditions avoid unphysical reflections that could strongly influence the flow in the vicinity of the airfoil.

2.3. *Finite volume discretization*

The Navier-Stokes equations are numerically solved on a grid that is too coarse to resolve all scales representing the turbulent fluid motion. The unavailable small-scale information, however, is crucial for the proper evolution of large-scale structures in the flow. Therefore, the effect on the resolved scales of their nonlinear interactions with the unresolved subgrid-scales (SGS) has to be represented by an SGS turbulence model.

Subgrid-scale models generally operate on flow scales that are marginally resolved by the underlying discretization scheme, i.e., the truncation error of common approximations for the convective terms can out-weigh the effect of even physically sound models. One can exploit this link by developing discretization methods where the truncation error itself functions as implicit SGS model. Approaches where SGS model and numerical discretization are merged are called implicit LES; refer to Ref. [15] for an introduction.

Representing a full merger of discretization and SGS model, the Adaptive Local Deconvolution Method (ALDM) has shown to be a reliable, accurate, and efficient method for implicit LES of Navier-Stokes turbulence [16, 17]. The implicit SGS model provided by this discretization can be interpreted as a combination of eddy-viscosity and scale similarity modeling. Model parameters were determined by a spectral-space analysis of the effective eddy viscosity in isotropic turbulence in the Reynolds numberÕs infinite limit by constraining the numerical dissipation to the physical SGS dissipation obtained from the analysis of nonlinear interactions in turbulence.

ALDM is used for discretizing the hyperbolic flux, whose discretization causes the SGS effects of interest, whereas standard centered differences are used for discretizing the viscous flux.

For time integration, the conditionally stable 3rd order Runge-Kutta method of Gottlieb and Shu [18] is used. This time-discretization scheme is total-variation diminishing (TVD) for $CFL \leq 1$, provided the underlying spatial discretization is TVD, whereas the linear stability bound is larger. As cut cell methods can generate cells with a very small fluid volume fraction, a special treatment of such cells is necessary when excessively small time steps according to the CFL stability criterion are to be avoided. For increasing the computational efficiency, we use a conservative mixing procedure, where the conservatives of small cells are mixed with larger neighbors [12,13]. During our simulations, the time step size is adjusted dynamically according to $CFL = 0.5$ based on the full cell size.

3. Results

The project has been initiated by performing first 2-D simulations and the results reported here are restricted to 2-D cases. All simulation were performed using ALDM and standard values of relevant parameters. It should be noted that, by design, ALDM provides a consistent SGS turbulence model for 3-D turbulence. In two dimensional or laminar flows ALDM does not provide a turbulence model but merely acts as a slightly

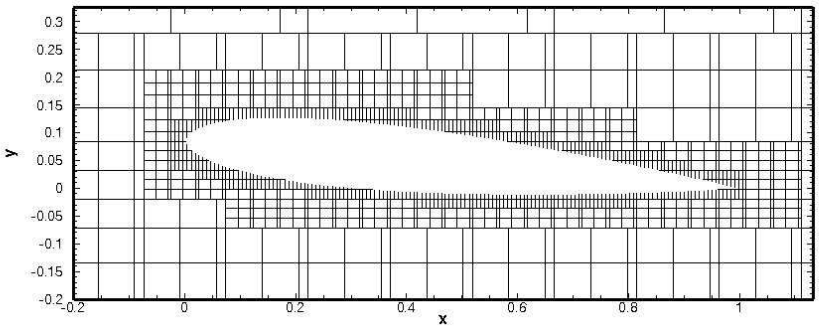

(a) Airfoil geometry and grid.

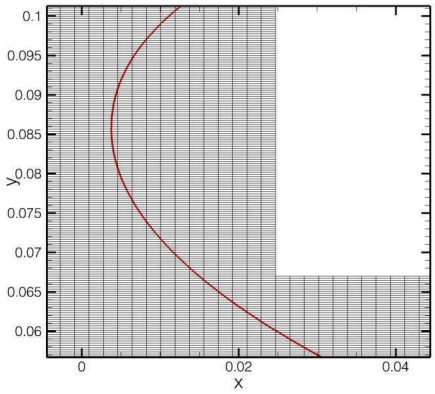

(b) Grid details at the leading edge of the airfoil.

FIGURE 2. Flow domain with a view of a computational grid.

dissipative, 2nd order accurate centered discretization. Therefore, the results presented below should be considered as DNS results.

3.1. *Geometry*

The geometry of the NACA-0012 airfoil at 5 deg of incidence and the computational grid are shown in Fig. 2. Two dimensional Cartesian grid has been generated through an adaptive mesh refinement procedure and two different resolutions were used, coarse with the total number of $64,827$ cells and fine with $128,142$ cells. For comparison, the baseline 2-D case of Jones *et al.* [6] used 1.6×10^6 grid points.

3.2. *Numerical simulations*

The flow has been simulated for around 13 time units, c/U, where c is the airfoil cord and U the free stream velocity. The equations of motion have been nondimensionalized using c and U, therefore in the results shown $c = 1$ and $U = 1$. Because of the low Mach number, the timestep had to be set to a low value of $\Delta t = 0.2 \times 10^{-4}$ which is a factor of 5 smaller than used by Jones *et al.* [6]. Appropriate boundary conditions must be applied to avoid unphysical reflections from the computational boundaries which could strongly influence the flow in the vicinity of the airfoil. Characteristic boundary conditions of Poinsot and Lele [14] are applied at all boundaries. At the downstream exit

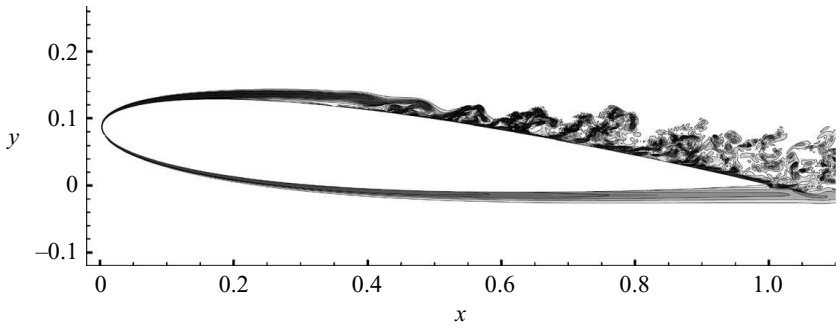

(a) Isocontours of vorticity in 3-D simulations of Jones *et al.* [6].

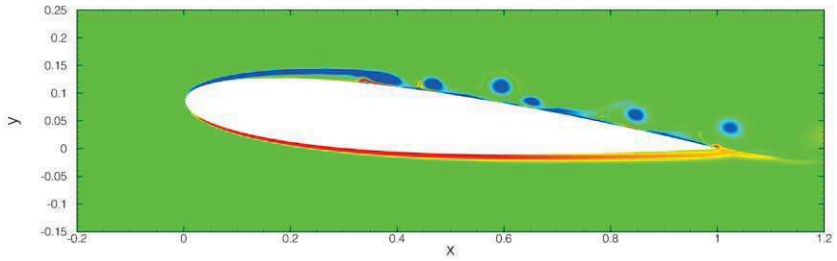

(b) Isocontours of vorticity in the present 2-D simulations.

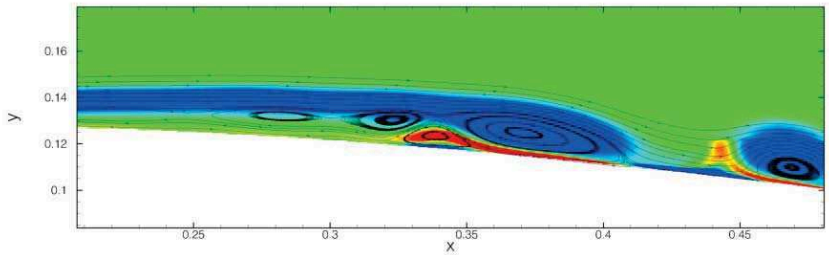

(c) Isocontours of vorticity in the vicinity of the separation point in the present 2-D simulations.

FIGURE 3. The vorticity field.

boundary, which is subject to the passage of nonlinear fluid structures, a lower value for the reflection parameter constant has been chosen in order to avoid pressure waves reflection into the computational domain.

The instantaneous vorticity field of the simulated flow is shown in Fig. 3 where it can be compared with the results of Jones *et al.* [6]. The present 2-D simulations capture qualitatively features observed in high resolution DNS, including the presence of a separated flow.

The quantitative assessment of the results is made by comparing in Fig. 4 the pressure and friction coefficients from our simulations with the corresponding data of Jones *et al.* [6] for their high resolution 2-D DNS case. The comparison for the pressure coefficient is quite good, especially on the pressure side of the airfoil. However, the comparison for the friction coefficient is poor overall. One important feature that appears to be predicted relatively well is the location of the initial separation point, signified by the transition in C_f from the positive to negative values on the suction side of the airfoil.

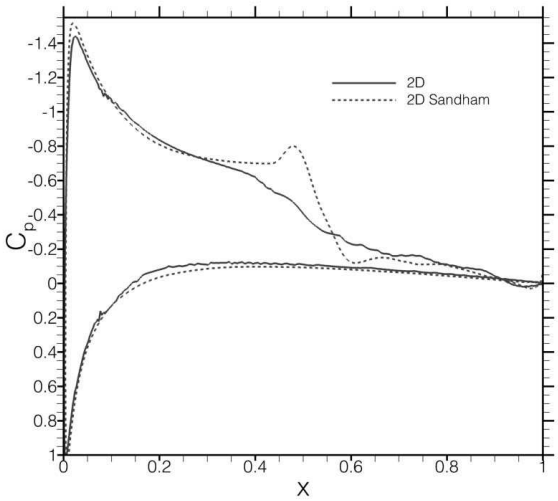

(a) Pressure coefficient comparison.

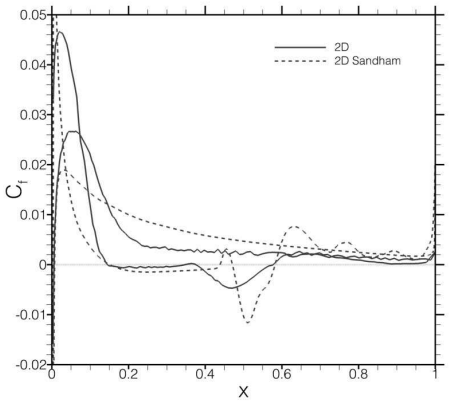

(b) Friction coefficient comparison - coarse resolution.

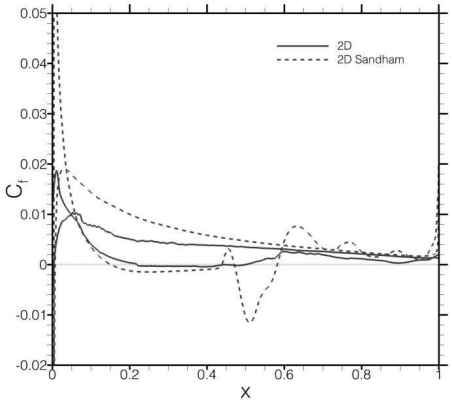

(c) Friction coefficient comparison - fine resolution.

FIGURE 4. Pressure and friction coefficients.

However, the simulations do not predict properly the secondary separation region at the mid-cord.

4. Conclusions

We have initiated a project to apply and evaluate LES techniques to simulate separated flows with *resolution reduced drastically from that used in DNS and typical LES performed for such problems*, the reduction target being a factor of at least 100. As the first step toward this goal we have adapted the code developed at TUM that uses immersed boundary method to simulate a flow around NACA-0012 airfoil for which a detailed DNS database is available [6]. While the code is fully three dimensional so far only 2D simulations have been performed with two different numerical resolutions, both

still lower than used in [6]. Compared with these baseline 2D DNS results, our simulations reproduce correctly qualitative features of the flow such as the structure of the vorticity field and the presence of a separation. We also obtain a fairly good quantitative comparison for the pressure coefficient and the location of the primary separation point. However, the quantitative comparison for the friction coefficient is poor. In particular, the simulations have trouble predicting the secondary separation region at the mid-cord. Nevertheless, considering fairly low resolutions employed, we believe that this work has amply demonstrated the capabilities of the code to simulate separated flows and we are currently extending this research to simulating such 3-D flows in the LES framework.

Acknowledgments

Two co-authors (GC and JAD) gratefully acknowledge support for this project provided through SFB/TRR 40 Program and the hospitality of faculty and staff of the Lehrstuhl für Aerodynamik und Strömungsmechanik, Technische Universität München, during the Summer Program when this research was performed.

References

[1] HU, H., YANG, Z. AND IGARASHI, H. (2007). Aerodynamic hysteresis of a low-Reynolds-number airfoil. *J. Aircraft*, **44**, 2083–2086.

[2] HAIN, R., KÄHLER, C. J. AND RADESPIEL, R. (2000). Dynamics of laminar separation buubles at low-Reynolds-number aerofoils. *J. Fluid Mech.*, **630**, 129–153.

[3] SPEDDING, G. R. AND MCARTHUR, J. (2010). Span efficiencies of wings at low Reynolds numbers. *J. Aircraft*, **47**, 120–128.

[4] LIN, J. C. M. AND PAULEY, L. L. (1996). Low-Reynolds-number separation on an airfoil. *AIAA J.*, **34**, 1570–1577.

[5] ALAM, M. AND SANDHAM, N. D. (2000). Direct numerical simulation of 'short' laminar separation bubbles with turbulent reattachment. *J. Fluid Mech.*, **410**, 1–28.

[6] JONES, L. E., SANDBERG, R. D. AND SANDHAM, N. D. (2008). Direct numerical simulations of forced and unforced separation bubbles on an airfoil of incidence. *J. Fluid Mech.*, **602**, 175–207.

[7] JONES, L. E., SANDBERG, R. D. AND SANDHAM, N. D. (2010). Stability and receptivity characteristics of a laminar separation bubble on an airfoil. *J. Fluid Mech.*, **648**, 257–296.

[8] SPALART, P. R. AND STRELETS, M. K. (2000). Mechanisms of transition and heat transfer in a separation bubble. *J. Fluid Mech.*, **403**, 329–349.

[9] WILSON, P. G. AND PAULEY, L. L. (1998). Two- and three-dimensional large-eddy simulations of a transitional separation bubble. *Phys. Fluids*, **10**, 2932–2940.

[10] YANG, Z. AND VOKE, P. R. (2001). Large-eddy simulation of boundary-layer separation and transition at a change of surface curvature. *J. Fluid Mech.*, **439**, 305–333.

[11] EISENBACH, S. AND FRIEDRICH, R. (2008). Large-eddy simulation of flow separation on an airfoil at a high angle of attack and $Re = 10^5$ using Cartesian grids. *Theor. Comput. Fluid Dyn.*, **22**, 213–225.

[12] MEYER, M., DEVESA, A., HICKEL, S., HU, X. Y. AND ADAMS, N. A. (2010). A conservative immersed interface method for large-eddy simulation of incompressible flows. *J. Comput. Phys.*, **229**, 6300–6317.

[13] GRILLI, M., HICKEL, S., HU, X. Y., ADAMS, N. A. (2009). Conservative immersed boundary method for compressible flows. *Academy Colloquium on Immersed boundary methods: current status and future research directions*, Amsterdam, The Netherlands.

[14] POINSOT, T. J. AND LELE, S. K. (1992). Boundary Conditions for Direct Simulations of Compressible Viscous Flows. *J. Comput. Phys.*, **101**, 104–129.

[15] GRINSTEIN, F., MARGOLIN, L. AND RIDER, W. (2007). *Implicit Large Eddy Simulation: Computing Turbulent Flow Dynamics*. Cambridge University Press.

[16] HICKEL, S., ADAMS, N. A. AND DOMARADZKI, J. A. (2006). An adaptive local deconvolution method for implicit LES. *J. of Comput. Phys.*, **213**, 413–436.

[17] HICKEL, S. AND LARSSON, J. (2008). An adaptive local deconvolution model for compressible turbulence. In: *Proc. CTR Summer Program 2008*, 85–96.

[18] GOTTLIEB, S. AND SHU C.-W. (1998). Total variation diminishing Runge-Kutta schemes. *Math. Comput.*, **67**, 73–85.